Towards an Overall 3-D Vector Field Reconstruction via Discretization and a Linear Equations System

Chrysa D. Papadaniil, *Student Member, IEEE,* and Leontios J. Hadjileontiadis*, *Senior Member, IEEE*

***Abstract*— A tomographic method that efficiently reconstructs three-dimensional fields, despite the ill-posedness of recovering a vector field from line integrals, is presented in this paper. The analysis takes into consideration the methodology set forth in [1] for 2-D reconstruction and demonstrates that with the analogous discretization of the 3-D space and scanning lines, data redundancy is achieved and the solution is obtained from a linear equations system solution, using only information from finite boundary measurements. The adequacy of the method is illustrated by means of simulations on electrostatic fields. The motivation behind this work lies in its potential to bring forward an alternative brain mapping model from EEG recordings.**

I. Introduction

Vector field tomography constitutes the methods used for the reconstruction of a field from integral data. Recovering a scalar field is a well posed problem and widely used in biomedical and other applications, e.g., X-ray measurements, Positron Emission Tomography (PET), seismic tomography. However, several applications, such as blood flow imaging, oceanography and photoelasticity, require the recovery of a field with 2-D or 3-D components, a problem that is, by definition, ill-posed. Mathematically, when integrating along a line, the vector field tomography formula is summarized

$$I_L = \int_L \bar{\mathbf{f}} \cdot \mathrm{d}\mathbf{s}, \tag{1}$$

where $\bar{\mathbf{f}}$ is the unknown field and $\mathrm{d}\mathbf{s}$ denotes the direction of the line L. For a two dimensional field, (1) coincides with the Radon transform and can be analyzed in

$$I_L = \int_L (f_x \cos w\hat{\mathbf{x}} + f_y \sin w\hat{\mathbf{y}})\mathrm{d}s, \tag{2}$$

while in three dimensions it coincides with the ray transform (the Radon transform integrating over planes),

$$I_L = \int_L (f_x \cos\phi \sin\theta\hat{\mathbf{x}} + f_y \sin\phi \sin\theta\hat{\mathbf{y}} + f_z \cos\theta\hat{\mathbf{z}})\mathrm{d}s. \tag{3}$$

In the equations above, f_x, f_y and f_z are the components of the 2 or 3 dimensional field, w is the angle of the line L with respect to the positive x-axis and ϕ, θ are the spherical angles of the line.

Studies on the ill-conditioning of the inverse vector field tomographic reconstruction have showed that a unique solution can be reached provided that specific constraints and assumptions are met. Hence, Norton initially achieved the recovery of the solenoidal component of a vector field, and later both solenoidal and irrotational components in the case of a divergenceless field [7], [8]. Braun and Hauck [9] suggested both longitudinal and transversal measurements for the full recovery of a vector field, a methodology that was later extended to three dimensions by Osman and Prince [10]. Yet, there are not many applications that make available both types of measurements.

Asterisk indicates corresponding author.

C. D. Papadaniil is with the Department of Electrical and Computer Engineering, Aristotle University of Thessaloniki, GR 54006 Thessaloniki, Greece, (e-mail: chrysa.papadaniil@gmail.com).

*L. J. Hadjileontiadis is with the Department of Electrical and Computer Engineering, Aristotle University of Thessaloniki, GR 54006 Thessaloniki, Greece, (e-mail: leontios@auth.gr).

II. Method Background and Potential

It was firstly suggested in [1] that a solution to the ill-posedness of a non-scalar field tomographic reconstruction problem could be the analysis in the digital domain, i.e., the discretization of both the field domain and the line integrals. In particular, to retrieve a two-dimensional field $\bar{\mathbf{f}}(x,y)$ in a bounded square domain, the domain is divided into finite tiles and the centers of the tiles are used as the points for the numerical vector field reconstruction. Then, ideal sensors are assumed, positioned at the middle points of the boundary edges of all boundary tiles. The line segments connecting all sensors apart from the ones lying on the same side are also sampled with a step Δs, the coordinates of the sampling points are calculated and assigned to the nearest tile center. Moreover, the angle w that defines the direction of each line, is taken into account and used in the numerical sum approximations to the line integrals. The equations develop an overdetermined linear system, the solution to which is given by the least squares method [12].

On the grounds that the solution of the derived system is in correspondence with the inversion of the Radon transform, the next works focused on reconstructing a vector field while satisfying the Radon transform requirements [3], [4]. These postulate that in order to acquire efficiently accurate medical image reconstruction, the Radon domain parameters need to be sampled densely and uniformly [6]. To this end, to compensate for the empirical sensor distribution of [1], virtual sensors that correspond to uniform sensor positioning were proposed in [3], where the values of the virtual sensors are calculated via interpolation schemes. Later, an improved method was presented in [4], where probabilistic weights are employed to achieve approximate uniformity. The applied sensor positioning results in a joint probability density function for the Radon parameters, which is then used to calculate the weight for every equation of the linear system. Hence, the equations are divided by their corresponding weights and multiplied with the pdf that uniform sampling would produce, leading to a more accurate reconstruction. Further,

978-1-4799-3163-7/13/$31.00 ©2013 IEEE

resolution issues were adressed in [2], where the sampling bounds for the Radon parameters were set for the optimized recovery of the 2-D vector field components.

The final goal for this recently developed methodology is to propose an alternative, direct solution to the inverse brain source localization problem from electroencephalography (EEG) measurements, other than the standard dipole-modelling or bayesian estimation techniques that are currently employed [11]. Reconstructing the bioelectric field inside the brain can be viewed as a representation of the brain state. Indeed, the psysical properties of this field conform to the assumptions adopted in the introduced reconstruction method. To this direction, it was showed in [5] that for the recovery of a two-dimensional, irrotational field, the discretization in the analysis constitutes a regularization technique for the under-determined problem in the continuous domain, by establishing a finite upper bound to the solution error. The method introduced here aims to extend the vector field reconstruction method straightforwardly to three dimensions, in a simple impementation that will serve as a basis for the adjustment of the method to fit the demands of the inverse EEG problem.

III. Proposed Reconstruction Method

Let us consider the three-dimensional vector field $\bar{\mathbf{f}}(x,y,z)$ in a bounded, cubic space, as in Fig. 1, with the start being at the center of the domain. The idea is to overcome the ill-conditioning of the reconstruction problem and to create data sufficiency by recovering all three components of the vector field f_x, f_y, f_z on specific sampling points of the space, using many line integral measurements. To this end, the cubic space is digitized to form a grid of $P\times P\times P$ tiles, the centers of which are taken to serve as the sampling reconstruction points. Presuming that the edges length is equal to $2U$, $2U/P$ has to be an integer. A line cutting across the domain, e.g., the segment AB of Fig. 1, is then assumed, with the intersecting points, A, B having the coordinates x_A, y_A, z_A and x_B, y_B, z_B, respectively. Based on spherical geometry, the line segment parameters are obtained by

$$r=\sqrt{(x_B-x_A)^2+(y_B-y_A)^2+(z_B-z_A)^2}, \tag{4}$$

$$\phi=\arctan(\frac{y_B-y_A}{x_B-x_A}), \tag{5}$$

$$\theta=\arccos(\frac{z_B-z_A}{r}), \tag{6}$$

where r is the length, ϕ is the azimuthal angle and θ is the polar angle of the segment. The unit vector in the direction of the line is defined as

$$\hat{\mathbf{s}}=\cos\phi\sin\theta\hat{\mathbf{x}}+\sin\phi\sin\theta\hat{\mathbf{y}}+\cos\theta\hat{\mathbf{z}}. \tag{7}$$

Subsequently, using A as the initial point and with a step of Δs, a sampling of the line segment is carried out, an example of which is shown in Fig. 2. Every sampling point on the segment has then coordinates increased by

$$\Delta x=\Delta s\cos\phi\sin\theta,\ \Delta y=\Delta s\sin\phi\sin\theta,\ \Delta z=\Delta s\cos\theta. \tag{8}$$

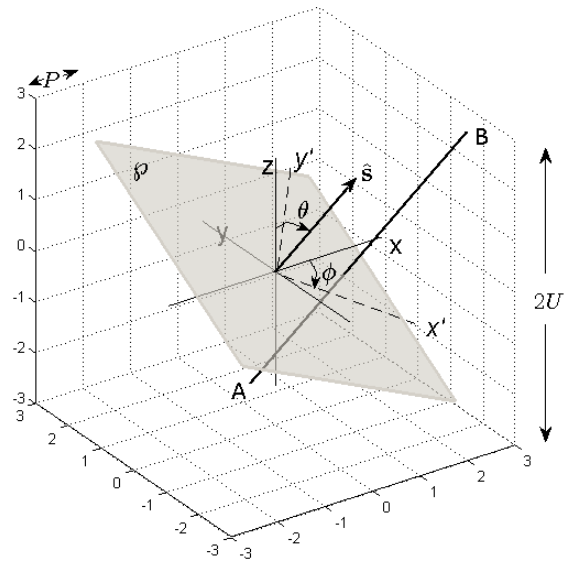

Fig. 1. A bounded cubic domain with edges equal to $2U$, divided into $P\times P\times P$ tiles. The view is limited to three faces of the domain for better visibility. A line segment AB, with direction vector $\hat{\mathbf{s}}$ crosses the domain. The plane $\wp$ is normal to $\hat{\mathbf{s}}$, while ϕ and θ are the azimuthal and polar angle, respectively.

Taking into account that the maximum number of sampling points that the segment can contain is given by

$$l_{AB}=\left\lfloor\frac{r}{\Delta s}\right\rfloor, \tag{9}$$

the coordinates of all the sampling points lengthwise for the segment AB are given by

$$x_l=x_A+l\Delta x,\ y_l=y_A+l\Delta y,\ z_l=z_A+l\Delta z, \tag{10}$$

where $l\in[1,l_{AB}]$. In order to achieve the requisite data sufficiency, each of these sampling points is assigned to the closest tile center by employing a proximal interpolation scheme

$$i=\left\lceil\frac{x_l+U}{P}\right\rceil,\ j=\left\lceil\frac{y_l+U}{P}\right\rceil,\ k=\left\lceil\frac{z_l+U}{P}\right\rceil. \tag{11}$$

The variables i, j, k suggest the integer enumeration of the digital space, an example of which is depicted in Fig. 2. Having acquired the reconstruction points that AB encloses information about, the next step is to numerically approximate AB 's line integral. Thus, the sum

$$I_{AB}=\sum\bar{\mathbf{f}}_{l_{i,j,k}}(x,y,z)\cdot\hat{\mathbf{s}}\,\Delta s \tag{12}$$

is used, where $\bar{\mathbf{f}}_{l_{i,j,k}}(x,y,z)$ stands for the towards reconstruction vector field values on the points with the discretized coordinates i, j, k, indicated by l, along the line AB.

For the formation of the method, assumtive sensors that will provide the boundary measurements are placed in the center of the outward faces of the border cubic tiles, as in Fig. 2. Following the procedure described for the lines that connect all the possible combinations of the boundary

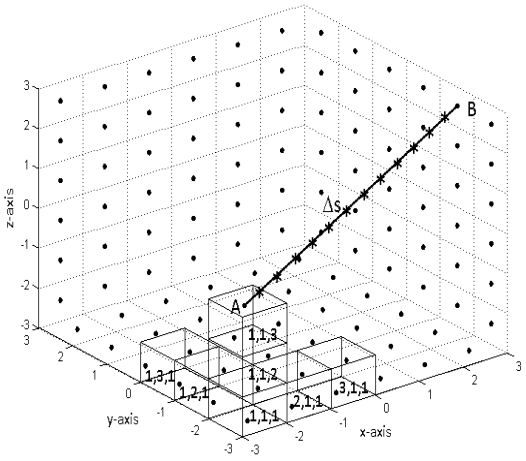

Fig. 2. The discretization of the cubic domain and of the *AB* scanning line segment of Fig. 1. Here, the circular markers on the centers of the boundary faces of the boundary tiles represent the sensor arrangement, as the asterisk markers symbolize the sampling points along *AB* with a step of Δs. The cubic tiles that are depicted show the (i, j, k) enumeration used, the rest of the tiles following the same pattern.

point sensors, excluding sensors that lie on the same face of the cubic space, a system of equations of the form (12) is yielded. Given that the unknown values of the vector field are

$$n = 3 \times \left(\frac{2U}{P}\right)^3, \tag{13}$$

while the number of the resulting equations is equal to

$$m = 15 \times \left(\frac{2U}{P}\right)^4, \tag{14}$$

the system can be synopsized in a structure of the form

$$\mathbf{b} = \mathbf{A}\mathbf{x}, \tag{15}$$

where $\mathbf{b}$ is the $m \times 1$vector that contains the sensors measurements, $\mathbf{x}$ is the $n \times 1$ vector that contains the measurements for the line integrals and $\mathbf{A}$ is the $m \times n$ system matrix, that contains the coefficients that associate each scanning line with the field values in the corresponding tiles. In addition, as $m > n$, the system is now well-conditioned and can be solved uniquely with the least squares method.

IV. Simulation Results

Following in the footsteps of [1]-[5], cases of an electrostatic field reconstruction were considered for the demonstration of the method. The field produced by electric monopoles is a suitable model for evaluation, as its irrotational property allows the estimation of the right part of the integral of (1) based on the difference of the voltage measurements between the two intersection points of the line with the domain. Thus, given the point sources, the vector b of the system was formed by calculating the voltage difference from all sensor couples. Using the methodology presented and the line orientation parameters, the coefficients of the matrix A were determined. As a result, the vector field components were retrieved using only boundary data.

Examples of reconstruction results using the proposed methodology are depicted in Fig. 3. In these examples, U was equal to 3 and P was taken equal to 1, leading to 216 cubic tiles. There were 3 unknown field components in every tile, thus the number of the unknows was 648. The abovementioned placement of the sensors gave rise to 19440 combinations, hence, 19440 equations, resulting in an over-determined system. The voltage values in these pretermined point were extracted using Coulomb 's law, while the sampling step along the lines was chosen to be 0.1. Finally, for comparison reasons, the theoretical field that the same point sources would cause was obtained with Coulomb' s law. In Fig. 3(i), the theoretical and reconstructed field were created by one point source placed at (11, 11, 11), while Fig. 3(ii) 's field was created by four point sources, with correspondent locations at (10, 10, 10), (-10, -10, -10), (10, 10, 0), (-10, -10, 0). In both cases Fig. 3(i) and Fig. 3(ii), subfigures with index (a) present the theoretical field, while those with (b) correspond to the reconstructed field. The relative magnitude error is demonstrated in subfigures with index (c) for every reconstruction point, while for (d) subfigures the angle difference between the two fields was calculated based on

$$\text{Angular Error} = \arccos\left(\frac{E_{xT}E_{xR} + E_{yT}E_{yR} + E_{zT}E_{zR}}{E_T E_R}\right), \tag{16}$$

where subscript T denotes the theoretical field and R denotes the reconstructed field. Thus, the numerator of (16) includes the three components of the fields, while the denominator includes their absolute values. Finally, in subfigures (e), (f) the histograms of the two kinds of errors are shown.

From the inspection of Fig. 3, the reconstructed fields are optically equivalent to the theoretical ones. Deviations from the theoretical field are anticipated, since the discretization process and the interpolation used for the sampling points assignment introduce errors. However, in the case of one source, the magnitude and angular errors are quite low, concentrating below 5% and 3°, respectively. In the case of Fig. 3.(ii), both errors are increased, especially in the boundaries of the y-axis, presumably because they lie closer to the sources' locations. The highest errors are seen in the magnitude values, while the orientation of the reconstructed field presents adequate similarity to the theoretical angles.

With a view to evade handling singularity issues, the point sources were, thus far, placed outside the bounded domain. It was observed, however, that the closer the sources are located, the more errors in magnitude and angle appear. In the examples presented, the condition number of the system matrices A was equal to 62.88, confirming a well-conditioned problem. In some cases of the grid being refined, the system is turning rank deficient. To this end, regularization and stability issues need to be adressed.

V. Conclusions and Future Work

In this paper, an extension of the vector field tomography method introduced in [1] and revisited in [2]-[5] to three dimensions was formulated. Whereas reconstruction

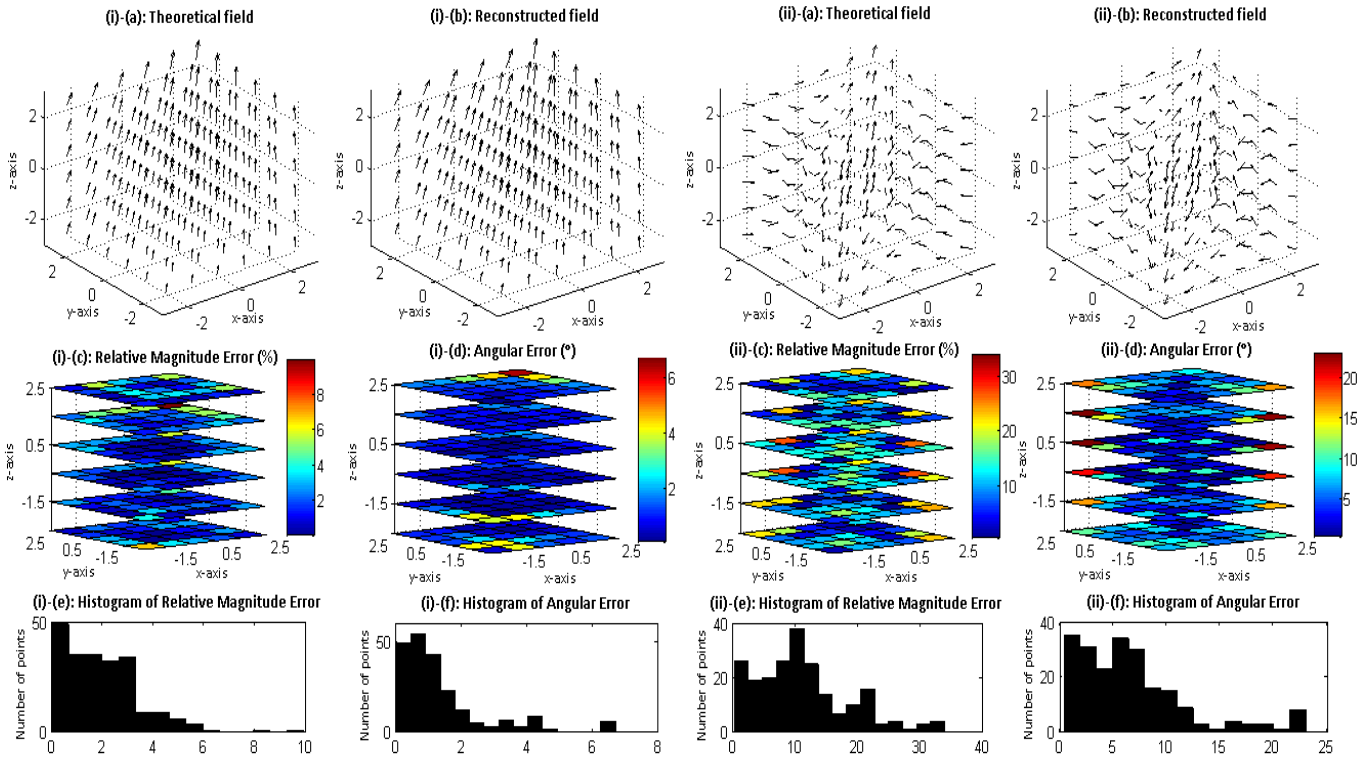

Fig. 3. Simulated examples and the performance of the proposed method. (i) One point source is placed at (11, 11, 11). (ii) Four point sources are placed at (10, 10, 10), (-10, -10, -10), (10, 10, 0) and (-10, -10, -10), respectively. In both cases (i) and (ii), (a) is the theoretical field calculated from Coulomb' s law, (b) is the reconstruction achieved by the method based on boundary data predetermined by Coulomb' s law, (c) shows the relative magnitude errors on the sampling points between (a) and (b) in slices of the z-axis and (d) shows the correspondent angular difference. Finally, the distributions of these errors are depicted in histograms (e) and (f), respectively.

of a vector field with two or three components based on integral data is considered an under-determined problem, the methodology adopted discretizes both the field domain and the scanning lines and recovers the unknown field in predetermined sampling points of the grid, thus generating data redundancy. The recovery depends only on boundary data and is derived as the solution of a linear sytem. The simulation results show that the method performs efficiently in 3-D, retrieving all three components of the unknown field.

Keeping in mind that the aimed application of the method is the EEG-based brain mapping problem, future work will include the stability issues already mentioned, as it is necessary for the method to be developed robustly, and the adjustment to more realistic head models. Following implementations also intend to incorporate more advanced techniques of discretizing the bounded 3-D domain. Finally, experiments with EEG data and comparisons with the current inverse EEG methods will need to be performed.

VI. Acknowledgements

This work was carried out as part of the GSRT Research Excellent Grant ARISTEIA, within the 4th Strategic Objective of the operational programme "Education and Lifelong Learning" entitled 'Supporting the Human Capital in order to Promote Research and Innovation', under grant agreement 440, project CBP: Cognitive Brain signal Processing lab, coordinated by the Information Technologies Institute - Centre for Research & Technology - Hellas.

References

[1] M. Petrou and A. Giannakidis, "Full Tomographic Reconstruction of 2-D Vector Fields using Discrete Integral Data", *The Computer Journal*, vol. 54(9), pp. 1491-1504, 2011.

[2] A. Giannakidis and M. Petrou, "Sampling bounds for 2D vector field tomography", *Journal of Mathematical Imaging and Vision*, Vol 37(2), pp 151-165, 2010.

[3] A. Giannakidis, L. Kotoulas and M. Petrou, "Virtual sensors for 2D vector field tomography", *Journal of the Optical Society of America A*, vol. 27(6), pp 1331-1341, 2010.

[4] A. Giannakidis and M. Petrou, "Improved 2D Vector Field Estimation using Probabilistic Weights", *Journal of the Optical Society of America A*, vol. 28(8), pp. 1620-1635, 2011.

[5] A. Koulouri and M. Petrou, "Vector Field Tomography: Reconstruction of an Irrotational Field in the Discrete Domain", *in Proc. SPPR*, 2012.

[6] S. R. Deans, *The Radon Tranform and Some of its Applications*, 2^{nd} edition, Malabar, Florida, Krieger Publishing Company, 1993.

[7] S. J. Norton, "Tomographic Reconstruction of 2D Vector Fields: Application to Flow Imaging", *Geophys. J. Int.*, vol. 97, pp.161-168, 1988.

[8] S. J. Norton, "Tomographic Reconstruction of 2D Vector Fields Using Boundary Data", *IEEE Trans. Image Process.*, vol. 1, pp. 406-412, 1992.

[9] H. Braun and A. Hauck, "Tomographic Reconstruction of Vector Fields", *IEEE Trans. Signal Process.*, vol. 39, pp. 464-471, 1991.

[10] N. F. Osman and J. L. Prince, "Reconstruction of Vector Fields in Bounded Domain Vector Tomography", *in Proc. IEEE-ICIP*, vol. 1, pp. 476-479, 1997.

[11] S. Baillet. J. C. Mosher and R. M. Leahy, "Electromagnetic Brain Mapping", *IEEE Signal Processing Magazine*, vol. 18, pp. 14-30, 2001.

[12] C. F. Gauss, *Theoria Motus Corporum Coelestium*, Perthes, Hamburg, 1809.